DESIGN AND EVALUATION
OF STAGGERED PARTITIONED PROCEDURES
FOR FLUID-STRUCTURE INTERACTION SIMULATIONS

Serge Piperno[1] and Charbel Farhat[2]

[1] CERMICS, INRIA, B.P. 93, 06902 Sophia-Antipolis Cedex, France.

[2] CAS, University of Colorado at Boulder, 80305 CO, USA.

Abstract

Numerical simulations of unsteady flows past a flexible structure require the simultaneous solution of structural dynamics and of fluid dynamics on deformable dynamic meshes. We present here an evaluation method of staggered partitioned procedures for time-integrating these focus coupled problems. This method is based on an estimation of the energy that is numerically created at the fluid/structure interface because of staggering. Simplifying assumptions make this estimation easy for a wide family of mixed explicit/implicit or implicit/implicit, synchronous or asynchronous procedures. Insights gained from this evaluation method are confirmed with the analysis of numerical results for the flutter of a flat panel in supersonic airstreams in two and three dimensions and for the transient aeroelastic response of an AGARD 445.6 wing in the transonic regime.

CONSTRUCTION ET EVALUATION DE PROCÉDURES DÉCALÉES
POUR LA SIMULATION D'INTERACTIONS FLUIDE-STRUCTURE

Résumé

La simulation numérique d'écoulements intationnaires autour de structures souples nécessite la résolution simultanée de problèmes de dynamique des structures et de dynamique des fluides en domaine déformable. Nous présentons ici une méthode d'évaluation d'algorithmes modulaires décalés utilisés pour l'intégration en temps de ce type de problème. Cette méthode repose sur une estimation de l'energie créée numériquement à l'interface fluide-structure à cause du décalage. Des hypothèses simplificatrices permettent d'évaluer simplement cette energie pour une grande famille d'algorithmes. Les prédictions obtenues par cette méthode ont été confirmées par l'analyse des résultats de simulations aéroélastiques du flottement d'un panneau soumis à un écoulement supersonique en deux et trois dimensions, et de la réponse instationnaire d'une aile AGARD 445.6 en régime transsonique.

1 Introduction

The numerical simulation of fluid/structure interaction phenomena arises in many aerospace engineering applications such as airfoil oscillations, flutter predictions, fighter tail buffeting, and a large class of other aeroelastic instability problems. Although closed-form solutions are available for aeroelastic computations when flows are not in the transonic regime, computational methods for complex nonlinear flows have been under development for almost twenty years [1]. These methods should be as efficient as possible (maximal time step for transient analysis). However, they should also predict accurately systems instabilities (the numerical diffusion - and then the time step - should be small), such that aircraft designer can rely on numerical simulations. Partitioned procedures for the transient analysis of fluid/structure interaction have become very popular and, more precisely, staggered procedures, for which Fluid Dynamics and Structural Dynamics are time integrated separately and successively. This kind of strategy allows modularity and computational efficiency through possible interfield parallelism [2].

In the past years, physical accuracy of transient numerical simulations was achieved by reducing the time step and as a side-effect the computational efficiency. The increase of machine performances was a partial solution to this problem. At the same time, some progress has been done towards the construction of accurate and efficient methods [3]. The role of energy and momentum exchanges through the fluid/structure interface has been emphasized. For example, the inconditional stability of some particular linear coupled system as well as true staggered procedure for these systems has been established, when some energy conservation property was assumed [4]. Furthermore, these ideas were translated to non-linear configurations, like the inviscid flow past a flexible structure, to improve the accuracy and stability properties of some partitioned procedures [5].

The aim of this paper is to construct a criterion for partitioned procedures giving an evaluation of the energy that is artificially created at the interface because of staggering. In order to make this evaluation easy, this energy is estimated under simplifying assumptions that might be dropped in further developements. An evaluation parameter is proposed for a wide family of staggered partitioned procedures (Section 2). These *a priori* estimations are then compared with numerical results of aeroelastic simulations in two- and three-dimensional configurations (Section 3).

2 Principles and description of the evaluation

In this section, we present the evaluation method for staggered partitioned procedures. These methods have been introduced to perform in a simple way numerical simulations of coupled problems. They computationally couple numerical methods for the interacting subsystems. However, the stability and accuracy of simple coupling algorithms are very different from those of numerical methods used in each decoupled field. In general, a much stronger condition on the time step is required. This explains why such computations can be very expensive.

It has been shown that the loss in accuracy and stability is due to staggering, because the forces and energies exchanged at the fluid/structure interface are not balanced [5]. Furthermore, a gain in accuracy and stability can be obtained if the differences between exchanged energies is controlled [5]. We propose here to construct an evaluation of the energy that is actually created at the interface because of staggering. We first compare the accumulated energies exchanged between the fluid and the structure for synchronous and asynchronous staggered procedures. Thereafter, we discuss the relative merits of each family of procedures as predicted by the

energetic evaluation.

We first fix some notation. In the following, U denotes structural displacements and a dotted symbol stands for the time-derivative of a quantity. We consider a generic point at the fluid/structure interface, and the corresponding boundary element. We omit the length or surface of this small element and the symbol P (for pressure) stands for a force as well (in the case of a viscous flow, the fluid force is not limited to the pressure force). Finally, superscripts are always related to the time, and the time step Δt is the structural time step.

2.1 Evaluation for a class of synchronous staggered schemes

We first consider the conventional serial staggered procedure (CSS) as introduced by Farhat *et al* [6]. This procedure is synchronous, i.e. the fluid and the structure are computed at the same times. In the following, we shall also consider the leap-frog type improved serial staggered procedure (ISS) of [6], which is clearly asynchronous. To make the description a little shorter, we now give the details of a generic staggered algorithm. For the staggered integration from t^n to $t^{n+1} = t^n + \Delta t$, the CSS prodecure reads

1. make a prediction X^{n+1} for the structural displacement at time t^{n+1}. In many studies, this prediction is completely outdated and reads $X^{n+1} = U^n$. We consider the more general prediction in function of parameters α_0 and α_1,

$$X^{n+1} = U^n + \alpha_0 \Delta t \dot{U}^n + \alpha_1 \Delta t \left(\dot{U}^n - \dot{U}^{n-1} \right) \tag{1}$$

2. compute a new fluid grid at time t^{n+1} matching this predicted displacement, and advance the fluid of Δt, possibly in a subcycled way (with as many fluid time steps as necessary). For subcycling, we have limited our investigations to algorithms for which the mesh speed is constant during a coupled time step. It is then given by $w^{n+1/2} = (X^{n+1} - X^n)/\Delta t$. This is the case for all procedures considered in [6], in which this choice was actually advocated.

3. compute a distribution of transferred fluid pressure forces P_S^{n+1} applied to the structure (with the time-averaging or time scheme of your choice). This force can be seen as the pressure force exerted by the fluid on the structure at time t^{n+1}.

4. advance the structure of Δt with the previously computed force.

The prediction (1) is first-order accurate if $\alpha_0 = 1$ and second-order accurate under the additional condition that $\alpha_1 = 1/2$. The fluid time-integration of step 2. can be done with explicit or implicit, first- or second-order accurate time schemes. In all cases, we can give an estimate for the transferred energy through an element of the fluid/structure interface. This estimate has the general form

$$\Delta E_F = - \left({}^T X^{n+1} - {}^T X^n \right) P_F^n, \tag{2}$$

where X denote successive displacements of the fluid grid boundary (coinciding with the prediction of the structural displacements) and P_F^n is the fluid pressure involved in the boundary flux for the current time-step. This formula is exact in one-dimension. P_F^n can take one of the

following values:

$$P_F^n = P^n \tag{3a}$$

$$P_F^n = P^{n+1} \tag{3b}$$

$$P_F^n \sim \frac{P^n + P^{n+1}}{2} \tag{3c}$$

$$P_F^n \sim \frac{1}{\Delta t} \int_{t^n}^{t^{n+1}} P(t) dt \tag{3d}$$

For example, for a first-order forward-Euler scheme, the energy flux through the fluid is computed using fluid values at time t^n. We then have $\Delta E_F = -\Delta t \, {}^T w^{n+1/2} P_n = \left({}^T X^{n+1} - {}^T X^n \right) P_n$. Then P_F^n is given by (3a). For an implicit backward-Euler scheme, P_F^n is given by (3b). This equation is only exact for true un-linearized implicit versions of the backward-Euler scheme. For second-order time schemes, a good approximation of P_F^n is given by (3c). Finally, we have considered the possibility of fluid subcycling. We assume the fluid grid is constant during all fluid subcycles of a coupled time-step. When the fluid time-step is sufficiently small compared to the structural time-step Δt, a second-order estimate of P_F^n is given by (3d).

Finally, in step 4., we assume the structure is linear and discretized using a finite element model yielding mass, damping and stiffness matrices M_s, D_s, and K_s (all three are symmetric positive, M_s and K_s being definite positive). It is time-advanced using the implicit trapezoidal rule, written in function of structural displacements U, velocities $V = \dot{U}$ and accelerations $A = \ddot{U}$, as

$$\begin{cases} U^{n+1} = U^n + \Delta t \frac{V^n + V^{n+1}}{2} \\ V^{n+1} = V^n + \Delta t \frac{A^n + A^{n+1}}{2} \\ M_s \, A^{n+1} + D_s \, V^{n+1} + K_s \, U^{n+1} = P_S^{n+1} \end{cases} \tag{4}$$

One fundamental property of the preceding trapezoidal rule concerns the energy received by the structure during one time step. We consider the structural energy

$$E_S = \frac{1}{2} {}^T V M_s V + \frac{1}{2} {}^T U K_s U, \tag{5}$$

then the structural energy variation during a time step is

$$E_S^{n+1} - E_S^n = \left(U^{n+1} - U^n \right) \frac{P_S^n + P_S^{n+1}}{2} - \Delta t . {}^T V^{n+1/2} D_s V^{n+1/2},$$

where $V^{n+1/2} = (V^n + V^{n+1})/2$. We can make a distinction between the energy lost by internal damping (negative term $-\Delta t . {}^T V^{n+1/2} D_s V^{n+1/2}$) and the energy transferred by the fluid

$$\Delta E_S = \left({}^T U^{n+1} - {}^T U^n \right) \frac{P_S^n + P_S^{n+1}}{2}. \tag{6}$$

Clearly, the exchanged energies (6) and (2) with P_F^n given by (3) cannot compensate exactly because the prediction (1) is not exact. Thus, energy is artificially created or dissipated at the fluide/structure interface. This could pollute numerical results of flutter simulations for example, and yield a poor accuracy in the determination of flutter limits.

In the sequel, we intend to give an evaluation of the artificial energy creation $\Delta E_F + \Delta E_S$ in the particular case where the structure is oscillating with a constant amplitude and pulsation

ω. We also assume that the fluid pressure on the structure oscillates with the same pulsation. For example, the two following coupled harmonic evolutions are possible :

$$\begin{cases} U(t) = \boldsymbol{U} \cos(\omega t) \\ P(t) = \boldsymbol{P} \cos(\omega t + \varphi) \end{cases} \qquad \begin{cases} U(t) = \boldsymbol{U} \cos(\omega t) \\ P(t) = M\ddot{U}(t) + D\dot{U}(t) + KU(t) \end{cases} \tag{7}$$

In (7), the first set of equations represents a simple phase shift between the fluid and the structure. In the second set of equations, aerodynamic loads on the structure have the effect of added mass, damping and stiffness matrices (respectively denoted by M, D and K). Both sets are equivalent if $\boldsymbol{P} \cos \varphi \equiv \left(K - \omega^2 M \right) \boldsymbol{U}$ and $\boldsymbol{P} \sin \varphi \equiv \omega D \boldsymbol{U}$. Let us define two parameters k and d by

$$k = {}^{T}\boldsymbol{U} \left(K - \omega^2 M \right) \boldsymbol{U} \equiv {}^{T}\boldsymbol{U} \boldsymbol{P} \cos \varphi, \quad d = {}^{T}\boldsymbol{U} \left(D\omega \right) \boldsymbol{U} \equiv {}^{T}\boldsymbol{U} \boldsymbol{P} \sin \varphi. \tag{8}$$

We assume systems are advanced in time using a constant time step Δt and successives values for U^n and P^n are then approximations of $U(t^n)$ and $P(t^n)$ with $T^n = n\Delta t$. Let us introduce the discretization parameter $h = \omega \Delta t$. Because of staggering, exchanged energies through the interface are not exactly opposite anymore. The error in energy exchanges depends on the global coupling algorithm. For example, let us assume we use the prediction (1) with $\alpha_0 = \alpha_1 = 0$ and an explicit forward-Euler scheme for the fluid with no subcycling, yielding a fluid energy variation given by (2) and (3a). Then for each time step,

$$\begin{aligned} \Delta E_F &= -\left({}^{T}U^n - {}^{T}U^{n-1} \right) P^n \\ &= \left[k \cos(\omega t^n) - d \sin(\omega t^n) \right] \left(\cos(\omega t^{n-1}) - \cos(\omega t^n) \right) \end{aligned}$$

The preceding formula is summed up over N coupled periods $T_\omega = 2\pi/\omega$ of oscillation. Using the lemmas,

$$\begin{cases} \sum_{NT_\omega} \cos(\omega t^n + c) \cos(\omega t^n) &\sim &\frac{N\pi}{h} \cos(c) \\ \sum_{NT_\omega} \sin(\omega t^n + c) \sin(\omega t^n) &\sim &\frac{N\pi}{h} \cos(c) \\ \sum_{NT_\omega} \sin(\omega t^n + c) \cos(\omega t^n) &\sim &\frac{N\pi}{h} \sin(c) \end{cases}, \tag{9}$$

the energy transferred to the fluid sums up to

$$\sum_{NT_\omega} \Delta E_F \sim N\pi \, \delta E_F \quad \text{with} \quad \delta E_F = \frac{1}{h} \left[k \left(\cos(h) - 1 \right) - d \sin(h) \right].$$

This term can be developped assuming $h \equiv \omega \Delta t \ll 1$ and takes the form

$$\delta E_F = -k \left(\frac{h}{2} - \frac{h^3}{24} \right) - d \left(1 - \frac{h^2}{6} \right) + O(h^4).$$

Similar elementary calculations can be done with the energy variation ΔE_S of (6) for any kind of scheme. For example, if we actually advance the structure before the fluid, i.e. with $P_S^{n+1} = P^n$, then we find that the energy transferred by the fluid to the structure sums up to

$$\sum_{NT_\omega} \Delta E_S \sim N\pi \, \delta E_S \quad \text{with} \quad \delta E_S = \frac{1}{h} d \sin(h) = d \left(1 - \frac{h^2}{6} \right) + O(h^4).$$

Thus, for this particular coupling algorithm, the total energy artificially created through the fluide/structure interface sums up to

$$\sum_{NT_\omega} \left(\Delta E_F + \Delta E_S \right) \sim N\pi \, \delta E \quad \text{with} \quad \delta E \sim -k \frac{h}{2}.$$

4

The parameter $\delta E \equiv \delta E_F + \delta E_S$ gives an evaluation of the accuracy of the coupling algorithm. Depending on the sign of k (and also the order of magnitude of k, which depends on the form of aerodynamic loads on the structure), this parameter can help predicting the behaviour of the scheme (artificial positive or negative damping) for small time steps ($h \equiv \omega \Delta t \ll 1$).

Let us emphasize the fact that evaluation parameters δE_F and δE_S can be computed separately for different fluid and structural parts of the coupling algorithms. In the following, we give the computed parameters for different schemes and discuss the merits of possible coupling algorithms in light of the parameter δE. In the sequel, we shall say that a coupling algorithm is n^{th}-order energy-accurate if $\delta E \sim C\, h^n$ when $h \rightarrow 0$ (and C is a constant).

2.2 Evaluation of δE_F for different fluid time schemes

We now give the values of δE_F for the general prediction (1) and different fluid time schemes, including those considered above and yielding fluid energy variation (2) with P_F^n given by (3). These values are given by

$$
\begin{aligned}
\delta E_F\,[(1)(3a)] \quad = \quad & k\left[(\alpha_0 - \frac{1}{2})h + (\frac{1}{24} - \frac{\alpha_0}{6} + \alpha_1)h^3\right] \\
& +d\left[-1 + (\frac{1}{6} - \frac{\alpha_0}{2} + \alpha_1)h^2\right] + O(h^4)
\end{aligned}
\tag{10a}
$$

$$
\begin{aligned}
\delta E_F\,[(1)(3b)] \quad = \quad & k\left[(\alpha_0 - \frac{3}{2})h + (\frac{5}{8} - \frac{7\alpha_0}{6} + 2\alpha_1)h^3\right] \\
& +d\left[-1 + (\frac{7}{6} - \frac{3\alpha_0}{2} + \alpha_1)h^2\right] + O(h^4)
\end{aligned}
\tag{10b}
$$

$$
\begin{aligned}
\delta E_F\,[(1)(3c)] \quad = \quad & k\left[(\alpha_0 - 1)h + (\frac{1}{3} - \frac{2\alpha_0}{3} + \frac{3\alpha_1}{2})h^3\right] \\
& +d\left[-1 + (\frac{2}{3} - \alpha_0 + \alpha_1)h^2\right] + O(h^4)
\end{aligned}
\tag{10c}
$$

$$
\begin{aligned}
\delta E_F\,[(1)(3d)] \quad = \quad & k\left[(\alpha_0 - 1)h + (\frac{1}{4} - \frac{7\alpha_0}{12} + \frac{3\alpha_1}{2})h^3\right] \\
& +d\left[-1 + (\frac{7}{12} - \alpha_0 + \alpha_1)h^2\right] + O(h^4)
\end{aligned}
\tag{10d}
$$

2.3 Evaluation of δE_S for different transferred forces P_S^{n+1}

We now give evaluations of the coefficient δE_S deriving from (6) and corresponding to different choices for the input forces P_S^{n+1} in the trapezoidal rule (4). We consider the four following choices:

$$
P_S^{n+1} = P^n
\tag{11a}
$$

$$
P_S^{n+1} = P^{n+1}
\tag{11b}
$$

$$
P_S^{n+1} = \frac{P^n + P^{n+1}}{2}
\tag{11c}
$$

$$
P_S^{n+1} = \frac{1}{\Delta t} \int_{t^n}^{t^{n+1}} P(t)dt
\tag{11d}
$$

For each choice of the form $P^\star$, we can compute a different input pressure force by determining the transferred force P_S^{n+1} verifying $\dfrac{P_S^n + P_S^{n+1}}{2} = P^\star$. This kind of algorithm gives an exact control of the momentum transferred by the fluid to the structure and partial control for the energy through (6). These additional choices correspond to

$$P_S^{n+1} = 2\ P^n - P_S^n \tag{12a}$$

$$P_S^{n+1} = 2\ P^{n+1} - P_S^n \tag{12b}$$

$$P_S^{n+1} = P^{n+1} \tag{12c}$$

$$P_S^{n+1} = \frac{2}{\Delta t} \int_{t^n}^{t^{n+1}} P(t)dt - P_S^n \tag{12d}$$

The reader can notice that choices (11b) and (12c) are strictly equivalent. We give developments of the parameter δE_S in function of h for these eight (actually seven) force inputs. Tedious calculations yield

$$\delta E_S\ [(11a)] \;\;=\;\; k\left[-\frac{h}{2} + \frac{h^3}{3}\right] + d\left[1 - \frac{2h^2}{3}\right] + O(h^4) \tag{13a}$$

$$\delta E_S\ [(11b/12c)] \;\;=\;\; d\left[1 - \frac{h^2}{6}\right] + O(h^4) \tag{13b}$$

$$\delta E_S\ [(11c)] \;\;=\;\; k\left[-\frac{h}{4} + \frac{h^3}{6}\right] + d\left[1 - \frac{5h^2}{12}\right] + O(h^4) \tag{13c}$$

$$\delta E_S\ [(11d)] \;\;=\;\; k\left[-\frac{h}{2} + \frac{h^3}{8}\right] + d\left[1 - \frac{h^2}{3}\right] + O(h^4) \tag{13d}$$

$$\delta E_S\ [(12a)] \;\;=\;\; k\left[-\frac{h}{2} + \frac{h^3}{24}\right] + d\left[1 - \frac{h^2}{6}\right] + O(h^4) \tag{13e}$$

$$\delta E_S\ [(12b)] \;\;=\;\; k\left[\frac{h}{2} - \frac{h^3}{24}\right] + d\left[1 - \frac{h^2}{6}\right] + O(h^4) \tag{13f}$$

$$\delta E_S\ [(12d)] \;\;=\;\; d\left[1 - \frac{h^2}{12}\right] + O(h^4) \tag{13g}$$

2.4   Discussion on δE for synchronous partitioned procedures

We first consider algorithms with $\alpha_0 = 0$ and $\alpha_1 = 0$ in the structural prediction (1). In that case, the prediction is only consistant. This kind of algorithm is first-order energy-accurate for all pair of schemes, excepted for the first-order explicit not-subcycled fluid scheme giving (3a) coupled with (12c). In that case, the error is almost zero since $\Delta E_F(t^{n-1} \to t^n) = -\Delta E_S(t^n \to t^{n+1})$. But this scheme is obviously not general.

We now consider first order predictions (1) with $\alpha_0 = 1$ and $\alpha_1 = 0$. Several algorithms in this class are second-order energy-accurate. Generally, the smallest error is obtained when exact exchange of momentum through the fluid/structure interface is achieved , i.e. when the force term in (12) corresponding to the fluid scheme is chosen. We get

$$\delta E\left[(1)_{\alpha_0=1}^{\alpha_1=1} - (3i) - (12i)\right] = -d\frac{h^2}{2} + O(h^3), \quad i = 1, \dots, 4. \tag{14}$$

However, the optimal scheme seems to be given by (3c) and 12d) for which the energy error is slightly smaller ($\delta E = -d\ 5h^2/12 + O(h^3)$).

Finally, the second order prediction (1) with $\alpha_0 = 1$ and $\alpha_1 = 1/2$ yields a third-order energy-accurate algorithm if and only if exact exchange of momentum through the fluid/structure interface is achieved. We get

$$\delta E \left[(1)_{\alpha_0=1}^{\alpha_1=1/2} \;-\; (3i) \;-\; (12i) \right] = k \frac{5h^3}{12} + O(h^4), \quad i = 1, \ldots, 4. \tag{15}$$

For the second-order prediction, the energy artificially created because of staggering is optimally reduced when the forces exchanged between the fluid and the structure at their interface are exactly opposed, and conservation of momentum is achieved. This happens when P_F^n and P_S^{n+1} respectively involved in (2) and (6) verify

$$P_F^n = \frac{P_S^n + P_S^{n+1}}{2}. \tag{16}$$

2.5 Evaluation for an asynchronous partitioned procedure

Farhat et al. [6] have advocated the use of the ISS asynchronous procedure. It is built as a leap-frog scheme (fluid values are computed at times $t^{n+1/2}$ and structural states at times t^n). The algorithm reads

1. compute the prediction $X^{n+1/2} = U^n + \frac{\Delta t}{2} \dot{U}^n$ (structural displacement at time $t^{n+1/2}$)

2. compute a new fluid grid at time $t^{n+1/2}$ matching this predicted displacement, and advance the fluid of Δt, possibly in a subcycled way.

3. compute a transferred fluid pressure distribution P_S^{n+1} applied to the structure.

4. advance the structure of Δt with the trapezoidal rule (4).

This procedure satisfies the Geometric Conservation Law (GCL) [7] without violating the interface continuity condition on velocities. This property is due to the trapezoidal rule, since $\dot{w}^n \equiv (X^{n+1/2} - X^{n-1/2})/\Delta t = (U^n - U^{n-1})/\Delta t + (\dot{U}^n - \dot{U}^{n-1})/2 \equiv \dot{U}^n$. The energy transferred to the fluid can again be written as $\Delta E_F = - \left({}^T X^{n+1/2} - {}^T X^{n-1/2} \right) P_F^n$, where

$$P_F^n = \bar{P} \tag{17}$$

and $\bar{P}$ takes one of the following values

$$\bar{P} = P^{n-1/2} \tag{18a}$$

$$\bar{P} = P^{n+1/2} \tag{18b}$$

$$\bar{P} \sim \frac{P^{n-1/2} + P^{n+1/2}}{2} \tag{18c}$$

$$\bar{P} \sim \frac{1}{\Delta t} \int_{t^{n-1/2}}^{t^{n+1/2}} P(t) dt \tag{18d}$$

corresponding respectively to a forward-Euler, a backward-Euler, a second-order implicit and a

7

highly-subcycled fluid scheme. For these choices, the parameter δE_F is then given by

$$\delta E_F\left[(17/18a)\right] \;=\; k\left[\frac{h}{2}-\frac{h^3}{48}\right]+d\left[-1+\frac{h^2}{24}\right]+O(h^4) \tag{19a}$$

$$\delta E_F\left[(17/18b)\right] \;=\; k\left[-\frac{h}{2}-\frac{h^3}{16}\right]+d\left[-1+\frac{h^2}{24}\right]+O(h^4) \tag{19b}$$

$$\delta E_F\left[(17/18c)\right] \;=\; k\left[-\frac{h^3}{24}\right]+d\left[-1+\frac{h^2}{24}\right]+O(h^4) \tag{19c}$$

$$\delta E_F\left[(17/18d)\right] \;=\; k\left[-\frac{h^3}{24}\right]+d\left[-1-\frac{h^2}{24}\right]+O(h^4) \tag{19d}$$

Reciprocally, for each possibility for $\bar{P}$ in (18), the input force P_S^{n+1} for the trapezoidal rule (4) can be chosen according to one of the two following choices

$$P_S^{n+1} \;=\; \bar{P} \tag{20}$$
$$P_S^{n+1} \;=\; 2\,\bar{P}-P_S^n \tag{21}$$

We now give the corresponding parameter δE_S for all these pressure choices. They read

$$\delta E_S\left[(20/18a)\right] \;=\; k\left[-\frac{3h}{2}+\frac{13h^3}{16}\right]+d\left[1-\frac{31h^2}{24}\right]+O(h^4) \tag{22a}$$

$$\delta E_S\left[(20/18b)\right] \;=\; k\left[-\frac{h}{2}+\frac{5h^3}{48}\right]+d\left[1-\frac{7h^2}{24}\right]+O(h^4) \tag{22b}$$

$$\delta E_S\left[(20/18c)\right] \;=\; k\left[-h+\frac{11h^3}{24}\right]+d\left[1-\frac{19h^2}{24}\right]+O(h^4) \tag{22c}$$

$$\delta E_S\left[(20/18d)\right] \;=\; k\left[-h-\frac{3h^3}{8}\right]+d\left[1-\frac{17h^2}{24}\right]+O(h^4) \tag{22d}$$

$$\delta E_S\left[(21/18a)\right] \;=\; k\left[-h+\frac{5h^3}{24}\right]+d\left[1-\frac{13h^2}{24}\right]+O(h^4) \tag{23a}$$

$$\delta E_S\left[(21/18b)\right] \;=\; d\left[1-\frac{h^2}{24}\right]+O(h^4) \tag{23b}$$

$$\delta E_S\left[(21/18c)\right] \;=\; k\left[-\frac{h}{2}+\frac{5h^3}{48}\right]+d\left[1-\frac{7h^2}{24}\right]+O(h^4) \tag{23c}$$

$$\delta E_S\left[(21/18d)\right] \;=\; k\left[-\frac{h}{2}+\frac{h^3}{16}\right]+d\left[1-\frac{5h^2}{24}\right]+O(h^4) \tag{23d}$$

Amongst all possible combinations, very few give second- or third-order energy accuracy. A second-order energy-accurate algorithm is obtained for the fluid force (17/18a) with one of the input forces (20/18b), or (21/18c), or (21/18d); another possibility is the joint use of a highly subcycled fluid yielding (17/18d) and the input force (21/18b). In that last case, $\delta E = -d\ h^2/12 + O(h^3)$. The only third-order energy-accurate combination is defined by (17/18c) and (21/18b); it does not allow subcycling at all.

2.6   General comparison of partitioned procedures

The class of synchronous staggered schemes of section 2.1 seem to be very accurate when a second-order prediction for the structural displacements is used ($\alpha_0 = 1$ and $\alpha_1 = 1/2$ in

(1)). The fundamental result of the evaluation of these methods is that, for any fluid time scheme, there is a way to achieve high energy accuracy. More precisely, provided the forces exchanged between the fluid and the structure at their interface are exactly opposed (16), the coupling algorithm is at least third-order energy-accurate. This is valid for any time scheme (explicit/implicit, first- or second-order time-accurate, subcycled or not).

On the contrary, the proposed asynchronous staggered method described in section 2.5 can lead to a third-order energy error, but for some particular scheme combination. It is also difficult to find a general principle as above, explaining why some scheme combinations should yield less artificial energy production. However, this asynchronous procedure conserves velocity continuity at the interface, a property that was not taken into account by the evaluation introduced in this paper.

In the sequel, we discuss on two- and three-dimensional results the validity of the above evaluations. We compare, for most energy-accurate coupling schemes, the actual behaviour of coupling algorithms with the behaviour predicted using our evaluation method.

3 Numerical Results

3.1 Supersonic panel flutter (two-dimensional)

We consider the aeroelastic response of a flat panel with infinite aspect ratio in a supersonic airstream [8, 2]. The physical problem is only two-dimensional. The panel (Fig. 1) has one side exposed to an airstream and the other side to still air. The panel considered here has a length $L = 0.5 \ m$, a uniform thickness $h = 1.35 \ 10^{-3} \ m$, a Young modulus $E = 7.728 \ 10^{10} \ N/m^2$, a Poisson ratio $\nu = 0.33$ and a density $\rho_S = 2710 \ Kg/m^3$. It is clamped at both ends ($x = 0$ and $x = L$). The pressure of the still air under the panel is P_∞ (fluid pressure at infinity).

The fluid is inviscid. The boundary condition at the fluid/structure interface is a slip condition, while at infinity, the fluid is assumed constant (pressure $P_\infty = 25714 \ Pa$, density $\rho_\infty = 0.4 \ Kg \ m^{-3}$, user-set Mach number M_∞). The simplified analytical study on the linear instability of the panel [8] is based upon the shallow shell theory and a first-order approximation of the aerodynamic theory where the influence of three-dimensional aerodynamic effects is neglected (this approximation is valid for $M_\infty > 1.6$). When the structural vertical displacement U is small, the fluid pressure forces on the panel can be approximated as a function of U and its derivatives. The global aeroelastic equation then reads

$$\rho_S h \frac{\partial^2 U}{\partial t^2} + \frac{E h^3 / 12}{1 - \nu^2} \frac{\partial^4 U}{\partial x^4} = -\frac{\rho_\infty u_\infty^2}{\sqrt{M_\infty^2 - 1}} \frac{\partial U}{\partial x} - \frac{\rho_\infty u_\infty (M_\infty^2 - 2)}{(M_\infty^2 - 1)^{3/2}} \frac{\partial U}{\partial t} \qquad (24)$$

where u_∞ denotes the gas velocity at infinity. The boundary conditions for U at clamped ends write $U(0) = U(L) = \frac{\partial U}{\partial x}(0) = \frac{\partial U}{\partial x}(L) = 0$. Frequencies for coupled modes are computed, and the limit Mach number where an unstable coupled mode appear can be estimated with a method of resolution from Houbolt [9]. For the present data, an instability appears at $M_\infty = 2.27$ with a pulsation $\omega = 462 rad/s$.

Aerodynamic loads can be rewritten as added mass, damping and stiffness matrices M, D and K in the formalism of (7). They are given by

$$M = 0, \quad D = -\frac{\rho_\infty u_\infty (M_\infty^2 - 2)}{(M_\infty^2 - 1)^{3/2}} \boldsymbol{I}, \quad K = -\frac{\rho_\infty u_\infty^2}{\sqrt{M_\infty^2 - 1}} \frac{\boldsymbol{\partial}}{\boldsymbol{\partial x}}.$$

9
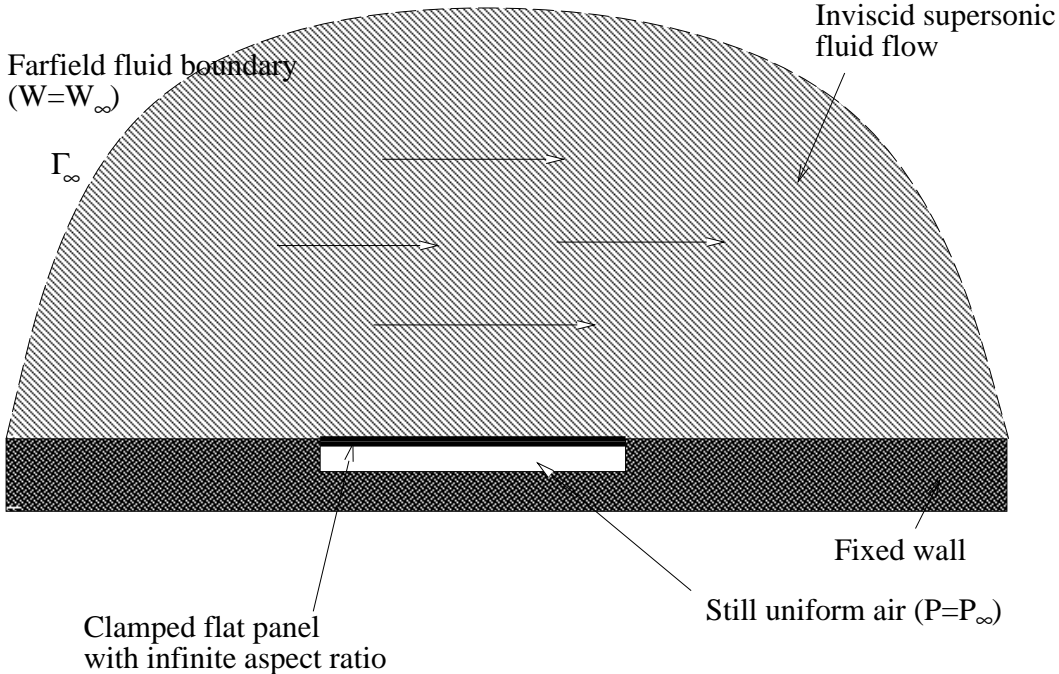
Figure 1: The flat panel with infinite aspect ratio.

We now assume the panel is not far from flutter. It oscillates with the pulsation $\omega = 462rad/s$ as in (7) and $\boldsymbol{U}$ is the flutter mode. Parameters k and d of (8) can be reduced to

$$
\left\{
\begin{array}{l}
k = -\dfrac{\rho_\infty u_\infty^2}{\sqrt{M_\infty^2 - 1}} \displaystyle\int_{x=0}^{L} \dfrac{\partial \boldsymbol{U}}{\partial x} \boldsymbol{U} \ dx, \\[4mm]
d = -\omega \dfrac{\rho_\infty u_\infty^2}{\sqrt{M_\infty^2 - 1}} \displaystyle\int_{x=0}^{L} \boldsymbol{U}^2 \ dx.
\end{array}
\right.
\tag{25}
$$

Note that k should equal zero since both panel ends are clamped. However, discretization errors and approximations in the aerodynamic theory make it only small.

For these computations a two-dimensional finite-volume method is used to solve the ALE-formulated inviscid Euler equations on a unstructured triangular grid with 1654 vertices and 2936 triangles. The convective fluxes are resolved by a MUSCL [10] second-order accurate Riemann solver on unstructured meshes [11, 12], for which an adapted version for ALE formulations was derived [13] . An explicit second-order Runge-Kutta scheme is used. Stability limitations lead to massive subcycling of the fluid. The structural operators are simply discretized using finite-differences with 299 vertices. The Mach number at infinity has been set to $M_\infty = 2.23$, which seems to be the flutter limit obtained for a reference run with the space discretizations used.

We consider the class of synchronous staggered schemes of Section 2.1. Heavy subcycling in the fluid and improved pressure forces (12d) transferred to the structure are used. The reference computation with no subcycling and $\Delta t = 1.23\mu s$ is compared with computations with $\Delta t = 200\mu s$ (which makes $\Delta t = T_\omega/70$ and $h \simeq 0.09$; the fluid is subcycled $n_{S/F} = 161$

times). We have chosen $\alpha_0 = 1$ in (1) and different values for α_1. We observe oscillations of the panel. To make the comparison simpler, we consider the scalar $\boldsymbol{x}$ defined by

$$\boldsymbol{x} = \rho_S\, h\ {}^T\!U_2 U,$$

where U is the panel displacement field and U_2 is the displacement field corresponding to the second structural eigenmode. The second modal coordinate $\boldsymbol{x}$ is shown on Figure 2 for these computations. The resulting curves give many qualitative and quantitative informations. First,
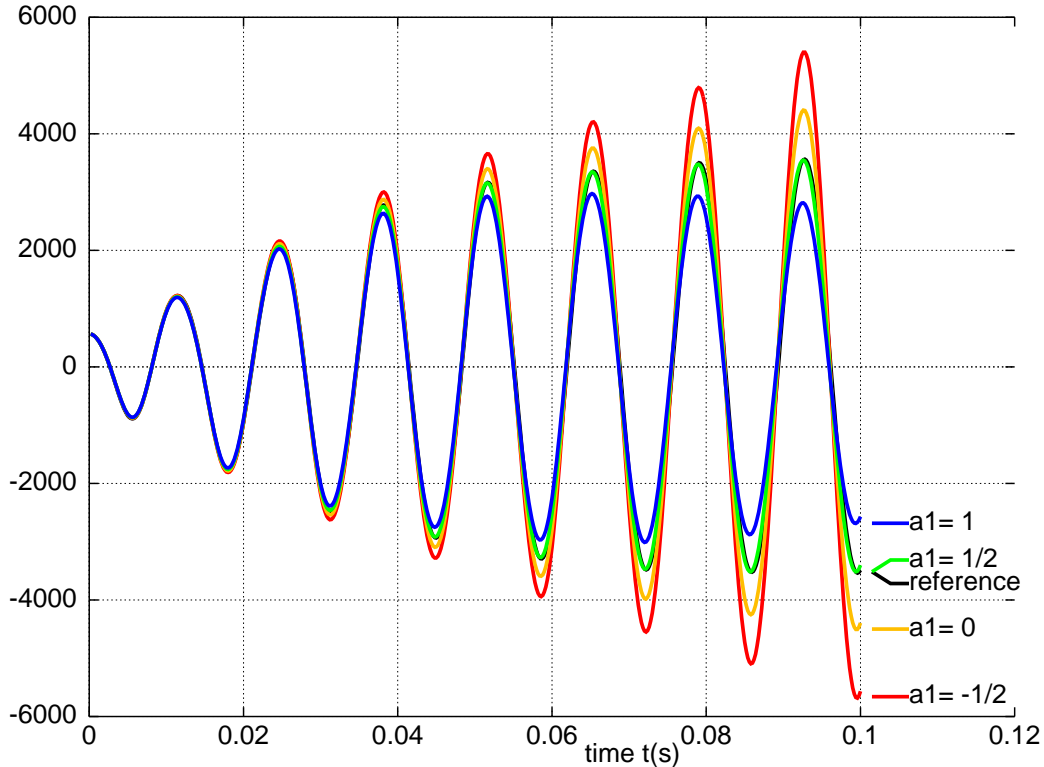
Figure 2: $\boldsymbol{x}$ computed with heavy subcycling ($n_{S/F} = 161$).

the qualitative (damped, stable, or undamped) behaviour of the panel differs from a run to another! The reference curve (and the almost coinciding curve obtained for $\alpha_1 = 1/2$) predicts the panel is exactly at flutter. Curves with $\alpha_1 = -1/2$ and $\alpha_1 = 1$ respectively predict that we are beyond and under the flutter limit.

Quantitatively, these curves confirm what could be deduced from (10d) and (13g). For a highly subcycled fluid and transferred pressure forces computed using (12d), the parameter δE corresponding to the energy artificially produced by staggering is estimated by

$$\delta E = \left(\alpha_1 - \frac{1}{2}\right) d\ h^2 + \frac{3}{2}\left(\alpha_1 - \frac{2}{9}\right) k\ h^3 + O(h^4), \tag{26}$$

(since $\alpha_0 = 1$). We can notice that the curve with $\alpha_1 = 1/2$ is matching the reference curve. Also, the deviation from the fixed amplitude oscillations seems to depend linearly on $\alpha_1 - 1/2$. Finally, schemes with $\alpha_1 > 1/2$ give artificially damped oscillations, because d in (25) is clearly negative. Reciprocally, schemes with $\alpha_1 < 1/2$ give artificially undamped oscillations.

We have also tested the asynchronous procedure defined by (17/18d) and (21/18b). The result is almost coinciding with the result of the method above with $\alpha_1 = 1/4$ (error $\delta E \sim$

11

$-dh^2/4$). However, our analysis predicts something smaller (error $\delta E \sim -dh^2/12$). This is probably due to the use of the value $P^{n+1/2}$ instead of a time integral (fluid high-frequencies are not filtered).

For $\alpha_1 = 1/2$ and $\Delta t = 200\mu s$, we have made an additional run with the transferred pressures (11d) instead of (12d). Values for the parameter $\boldsymbol{x}$ obtained with each choice of pressures are shown in Figure 3. The advantage of forces computed using the fromula (12d)
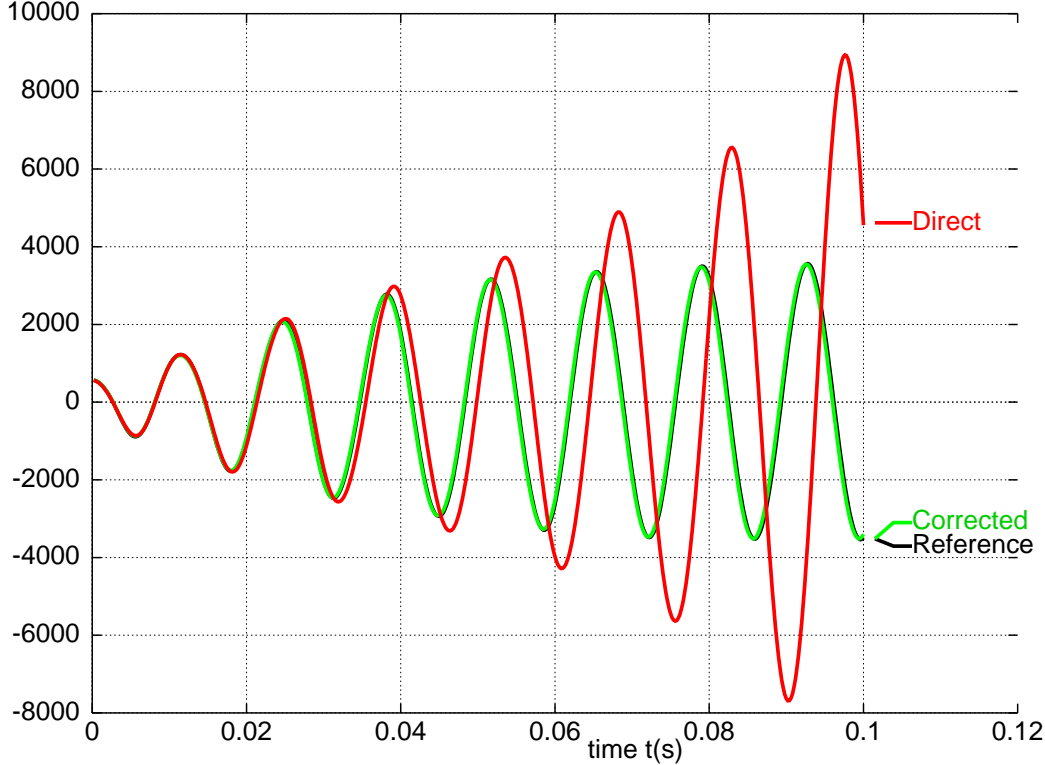
Figure 3: $\boldsymbol{x}$ computed with different transferred pressures.

instead of (11d) is clearly demonstrated. For this subcycling of $n_{S/F} = 161$, the error in force exchange at the interface produces negative artificial damping and phase shift. According to (10d) and (13d), the parameter δE for this algorithm is estimated by

$$\delta E = -\frac{1}{2} \; k \; h - \frac{1}{4} \; d \; h^2 + O(h^3). \tag{27}$$

This estimate is to be compared to $\delta E \sim (5/12)k \; h^3$ given by (26), which is roughly 150 times bigger!

Finally, we have tested massive fluid subcycling to reach the stability and accuracy limits of the coupling algorithm. We use the value $\alpha_1 = 1/2$. Values for $\boldsymbol{x}$ obtained for $\Delta t = 200\mu s$ ($\Delta t = T_\omega/70$, $h \simeq 0.09$, $n_{S/F} = 161$), $\Delta t = 400\mu s$ ($\Delta t = T_\omega/35$, $h \simeq 0.18$, $n_{S/F} = 322$) and $\Delta t = 600\mu s$ ($\Delta t = T_\omega/23$, $h \simeq 0.28$, $n_{S/F} = 482$) are shown in Figure 4. The algorithm is quite robust, since the curve with $\Delta t = T_\omega/35$ ($n_{S/F} = 322$) also coincides with the reference curve. However, the last computed solution is a little undamped ($n_{S/F} = 482$). We reach the limits of the proposed analysis, since $h \simeq 0.28$ is not really small. Altogether, the stability and accuracy limit of $\Delta t = T_\omega/35$ is quite reasonable for staggered partitioned procedures.
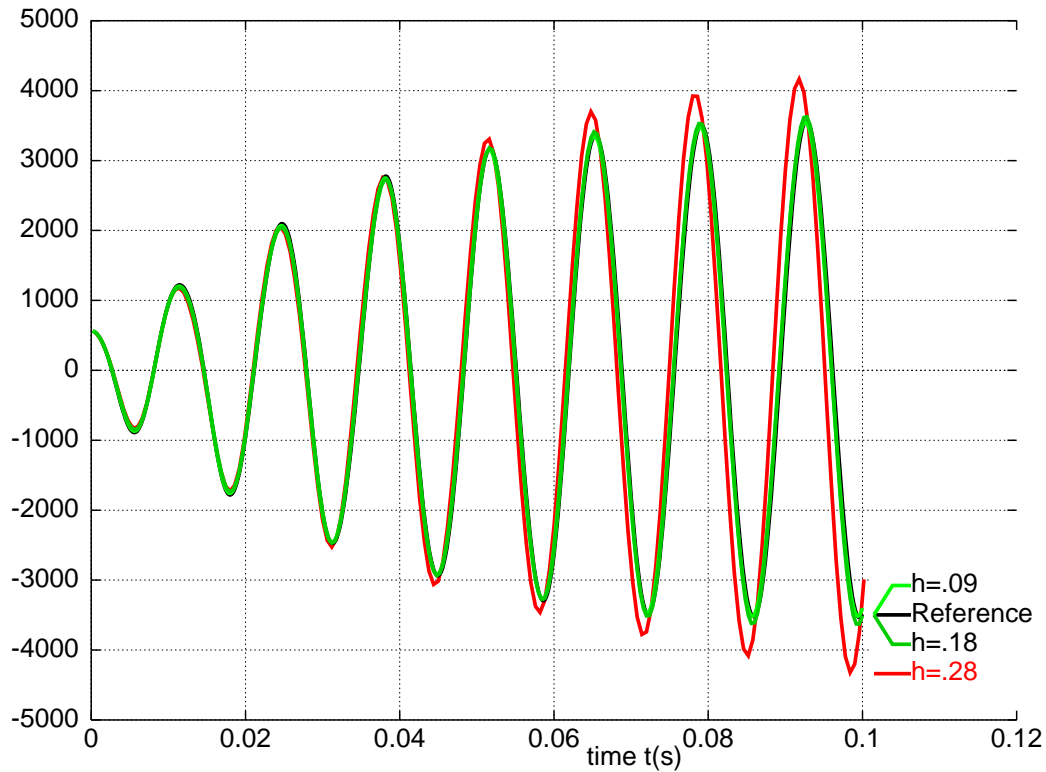
Figure 4: $\boldsymbol{x}$ computed with massive subcycling.

3.2 Supersonic panel flutter (three-dimensional)

In this section, we compare numerical results to qualitative predictions for the three-dimensional simulations of the supersonic flutter of a flat panel with infinite aspect ratio. The case is nearly the same as in the previous section and is detailed in [14]. The panel is now two-dimensional as shown on Figure 5. The panel is still clamped at both ends. The depth of the panel is fixed to
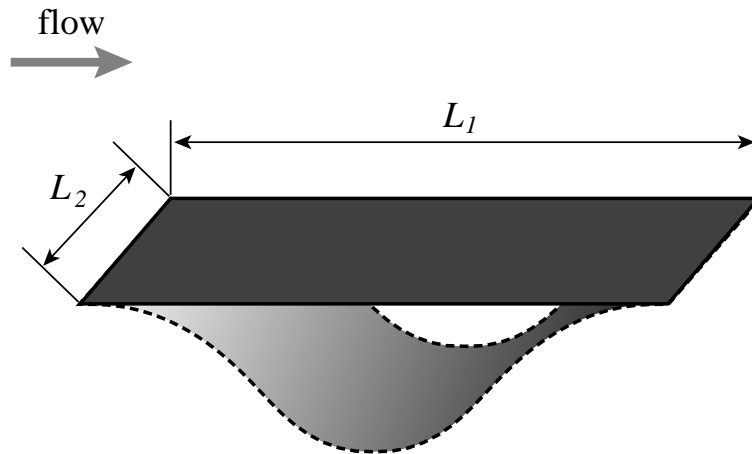
Figure 5: Initial perturbation of the two-dimensional flat panel.

$L_2 = 0.1$. The finite element structural model contains 100 triangular shell elements, 102 nodes, and 612 degrees of freedom. The flow domain above this panel is discretized into 20250 vertices

13

and 94080 unstructured tetrahedra. A slip condition is still imposed at the fluid/structure boundary. An implicit fluid solver is used in the sequel. The aeroelastic response of the coupled system is triggered by a displacement perturbation of the panel along its first bending mode (see Figure 5). However, we consider a time step equal to $\Delta t = 100 \mu s$, which gives a accurate sample for the three fundamental modes of the panel ($\Delta t \sim T_3/60$).

In a first series of runs, the Courant number is set to 10 in the implicit fluid code, and several partitioned procedures are applied to compute the transient aeroelastic response of the panel. The time step used induces no subcycling and a additional reference computation is performed using $\Delta t = 10 \mu s$. The obtained lift histories are depicted in Figure 6 for the first 0.1 physical seconds.
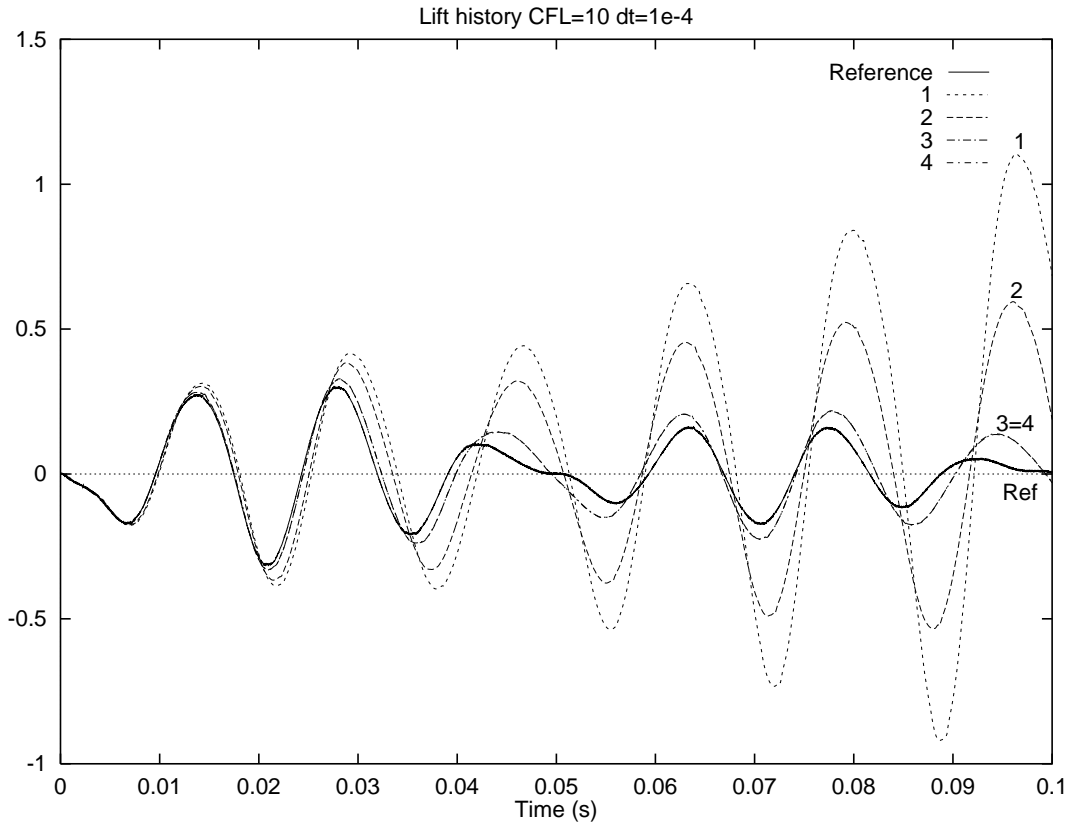
Figure 6: Lift histories for several procedures.

The most unstable curve (label 1) was obtained with the Conventional Parallel Staggered procedure (CPS, see [6]) : it is defined a synchronous procedure with $\alpha_0 = \alpha_1 = 0$ and exchanged forces are given by (3b) and (11b), respectively because the fluid time scheme is a first-order backward-Euler and because the structure could be integrated at the same time. For this algorithm, the energy parameter given by our evaluation is $\delta E = -2\ kh$. It should be compared with the Conventional Serial Staggered procedure (CSS) of [6], corresponding to the synchronous procedure with $\alpha_0 = \alpha_1 = 0$ and pressures forces (11a) on the structure (the structure is advanced after the fluid time step is completed). For the CSS procedure (label 2), we have $\delta E = -1.5\ kh$, which is in a relatively good agreement with the form of both curves in

Figure 6. We have also tested (label 3) the Improved Serial Staggered procedure (ISS) of [6], corresponding to the asynchronous method (17/18b) with force exchanges (21/18b). And finally, we had a run (label 4) with the synchronous procedure with the first-order prediction ($\alpha_0 = 1$, $\alpha_1 = 0$) and forces exchanges (3b) and (11b). Both curves coincide on Figure 6. For both, our analysis predicts $\delta E = -0.5\ kh$. The comparison of several partitioned procedures reveals that our evaluations are qualitatively and quantitatively in good agreement with numerical results.

In a second series of runs, we investigate the effects of subcycling. This analysis is performed on the ISS procedure. The evaluation parameter δE for (17) and exchange forces (21/18b) can be estimated for any subcycling factor $n_{S/F} = N$. We found $\delta E = -\frac{1}{2N}\ kh$. This dependence on $n_{S/F}$ is verified on numerical results for varying subcycling factors. In Figure 7, the curve with $n_{S/F} = 5$ is almost coinciding with the reference curve.
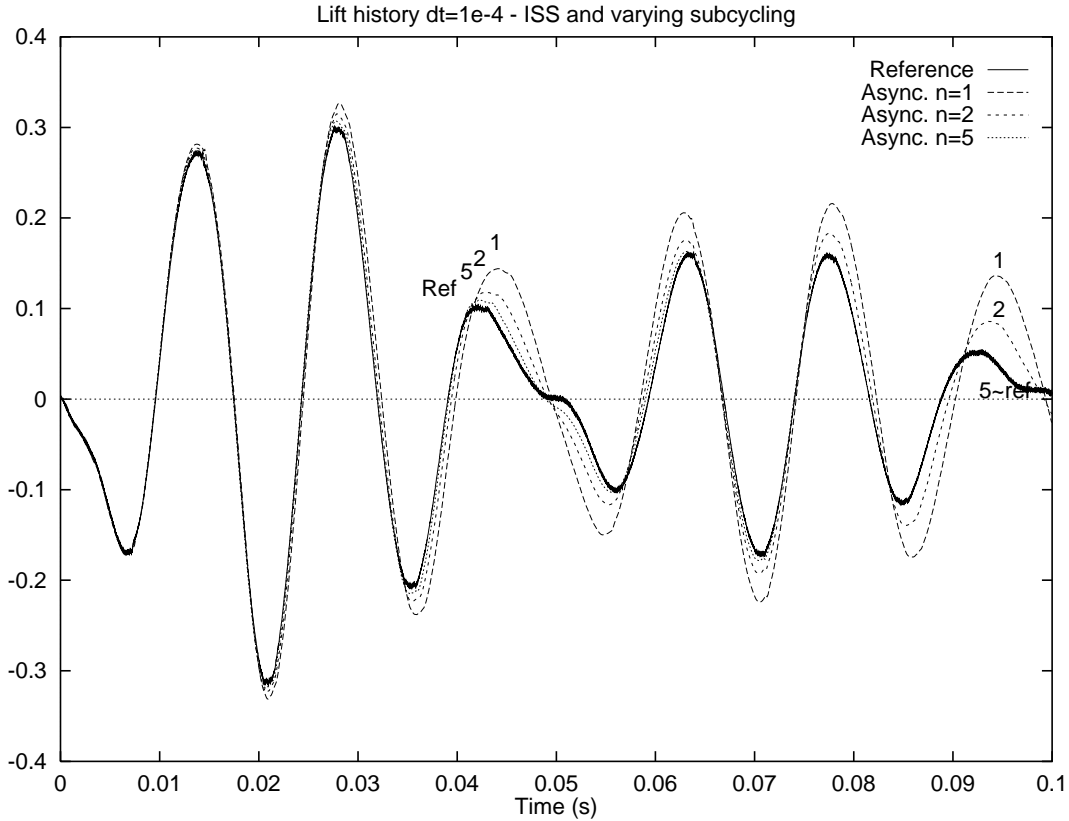
Figure 7: Dependence on the subcycling factor $n_{S/F}$.

Finally, we conduct a last series of run to compare the dependences on the coupled time step Δt and on the subcycling factor $n_{S/F}$. We have chosen the ISS procedure described above. The computed lift histories corresponding to $\Delta t = 100\mu s$ and $\Delta t = 300\mu s$ (labels 2 and 3 respectively) with no subcycling, and to $\Delta t = 300\mu s$ with $n_{S/F} = 3$ (label 4) are plotted in Figure 8. The comparison of curves (2) and (3) shows the amplification of oscillations as h was increased. But the linear dependence on h of the created energy does not appear clearly on the results. If the transmitted energy depends linearly on h, then the lift, pressure and displacements should vary like $\sqrt{h}$. However, the reference run itself is a bit far from the
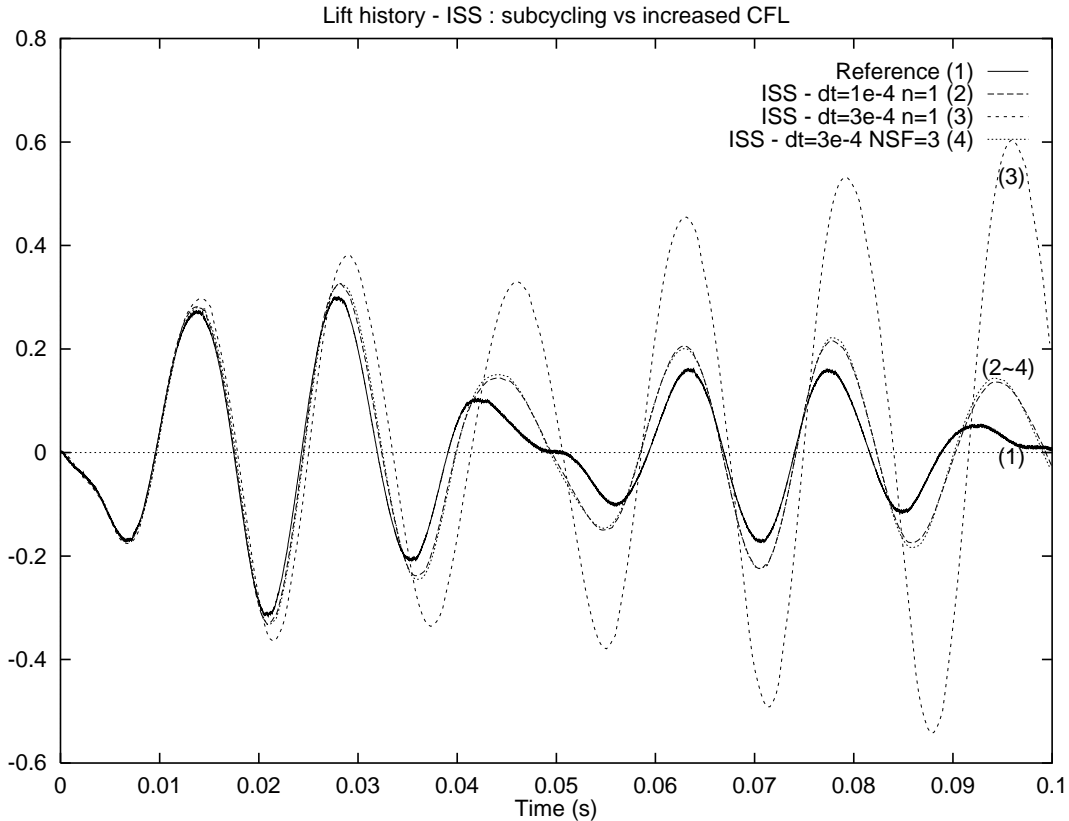
Figure 8: Dependence on Δt and $n_{S/F}$.

harmonic oscillation that is assumed in our evaluation. On the other hand, curves (2) and (4) are almost coinciding, and this was actually predicted by the evaluation (from (2) to (4), $h \rightarrow 3h$ and $n_{S/F} \rightarrow 3n_{S/F}$).

In conclusion, we have given an new interpretation to previously published numerical results on panel flutter simulations. The evaluation method we have proposed is in good agreement with numerical lift histories for several transient procedures. However, these procedures are only first-order energy-accurate and additional simulations should be performed to validate the proposed evaluation method.

3.3   Flutter analysis of the AGARD Wing 445.6

We finish this report with the analysis of numerical results obtained with some transient procedures for the flutter analysis of the AGARD Wing 445.6. This wing is fully described and referenced in [6]. The structure is discretized using a undamped finite element model with 800 triangular composite shell elements and 2646 degrees of freedom. It yields natural mode shapes (and frequencies) that are similar to those derived exprimentally. However, the flutter analysis is conducted using the true finite element representation of the wing. Numerical results presented here were obtained on a unstructured tetrahedral fluid mesh with 22014 vertices. Even though it is coarse, this CFD mesh has proved to be adequate for aeroelastic analysis. A partial view of this mesh is shown in Figure 9. The freestream conditions are set to $M_{\infty} = 0.901$, $\rho_{\infty} = 1.117 \ 10^{-7}$ slugs/in^3, and $p_{\infty} = 10$ slugs/(sec$^2 \times$ in). Fluid time-integration is carried out by a second-order implicit backward difference scheme whose implementation satisfies the

16
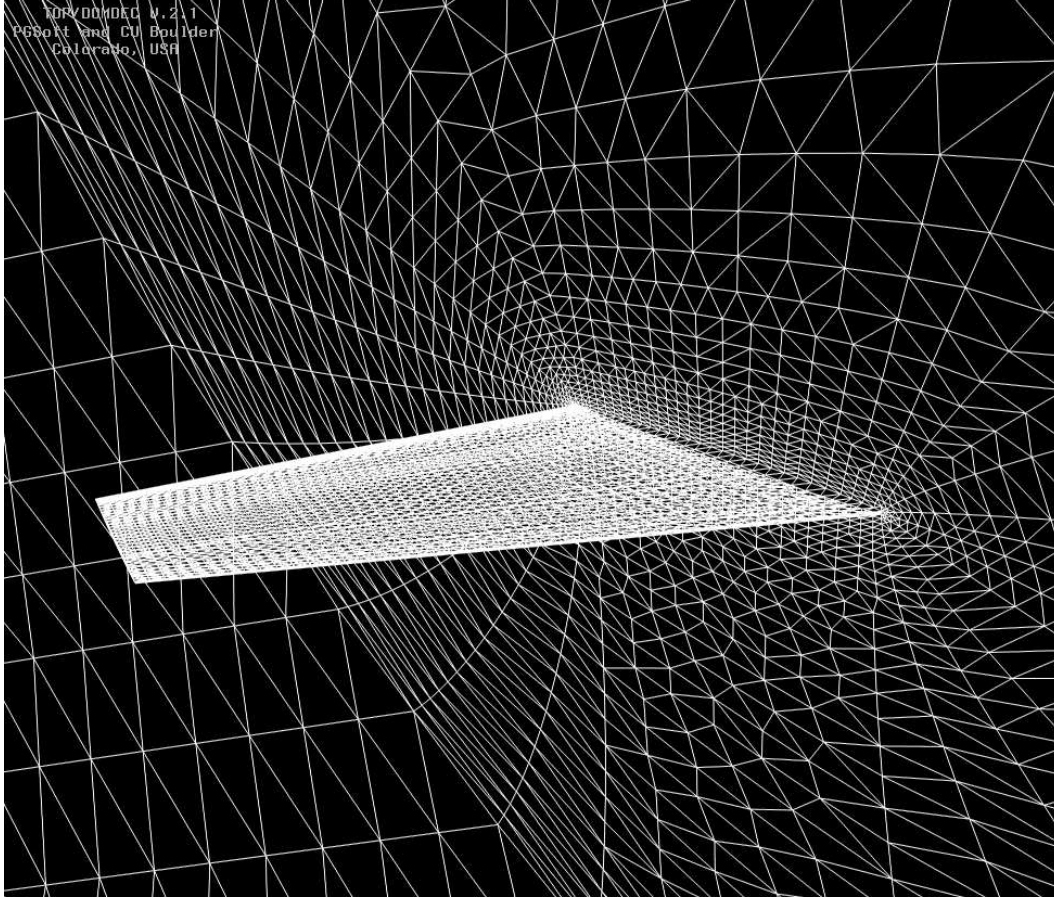
Figure 9: Partial view of the CFD mesh.

geometric conservation laws [15]. The fluid time-step has been set to $\Delta t_F = 0.5ms$.

The finite element structural model is perturbed along its first bending mode, a steady state solution is computed around the deformed configuration of the wing and finally the aeroelastic response is computed using some staggered partitioned procedure.

This case is the most difficult one. The flow is absolutely three-dimensional and is not smooth because of the transonic regime considered. Structural and fluid schemes are not conforming at the fluid/structure interface, and structural large displacements with possible rotations occur. Thus, we guess our evaluation method should give limited insights on the partitioned procedures. We also point out the fact that, in this case, the wing is far away from flutter, and the system is naturally damped. Thus, our method based on harmonic oscillations could give inaccurate predictions.

Since a second-order implicit backward difference scheme is used for the fluid, the ISS procedure has an increased accuracy (with no or light subcycling). Actually, our evaluation leads to $\Rightarrow \delta E = 1/16 \ dh^2$, which means that an order of accuracy in energy exchanges has been gained. We perform two series of runs to compare the ISS procedure to the less accurate CSS and CPS procedures (which are basically first-order).

Convergence of the lift history for the CSS procedure is plotted in Figure 10. In these computations, the default time-step is $\Delta t = 1ms$ (which yields two fluid subcycles per iteration).

17
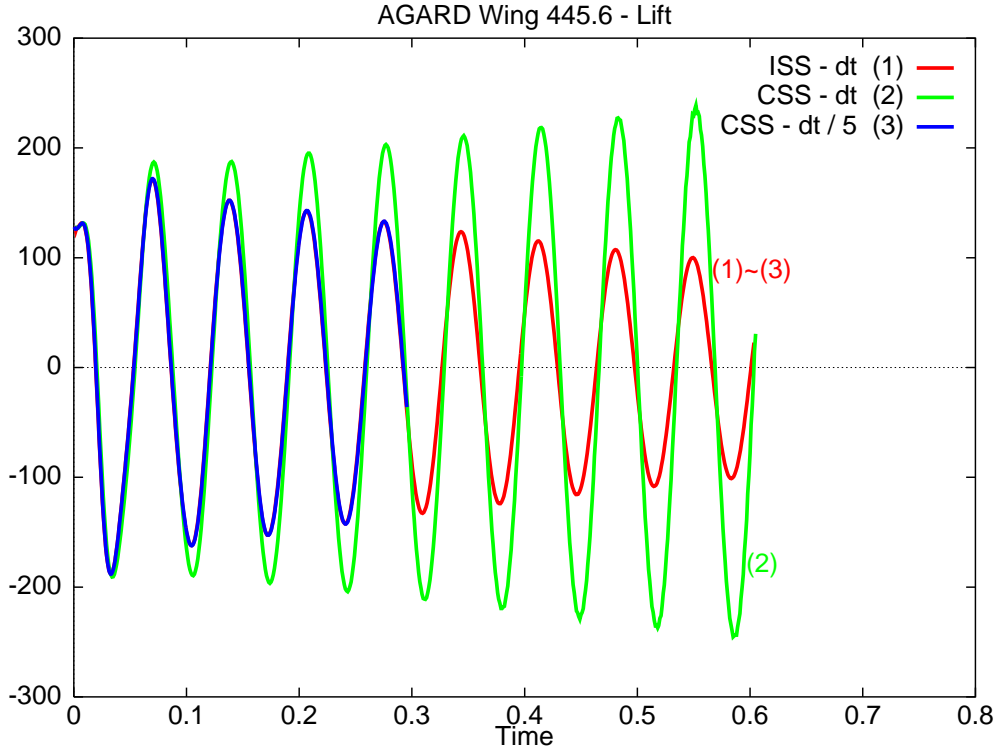
Figure 10: Comparison of lift histories with ISS and CSS.

The CSS method yields an undamped result for this time step, but converges to a correct result for $\Delta t = 0.2ms$ (the curve coincides with the ISS curve). These curves confirm the difference in order of energy accuracy between CSS and ISS. This difference can actually be converted into a gain in numerical stability and computational efficiency.

Similar results are shown in Figure 11 for the even less accuracte CPS procedure. The difference in order of energy accuracy between CSS and ISS is clearly verified. However, in the long run, the CPS seems to be much more unstable and inaccurate than predicted. This could be a consequence of the simplifying assumptions of the evaluation method, that could be not valid in this particular case with a non-smooth flow (transonic regime) and real three-dimensional effects (for both the flow and the discretizations).

4   Conclusion

In this report, we have proposed a new evaluation method for time schemes in partitioned procedures for fluid/structure interactions. This method yields a measure of the default of energy conservation through the fluid/structure interface. This measure is both qualitative (different orders of accuracy in energy conservation can be reached) and quantitative (coupling schemes with the same order of accuracy can be more precisely compared).

This method was validated on numerical results for aeroelastic responses of structures in both two- and three-dimensional configurations. The damped or undamped response of the structure, which results from numerical errors, has been reinterpreted in terms of energy accuracy and was accurately predicted by our evaluation technique.

However, this technique has strong limitations, since it is based on rather simple assumptions. We intend to investigate in our future works the possibility of extending the validity of
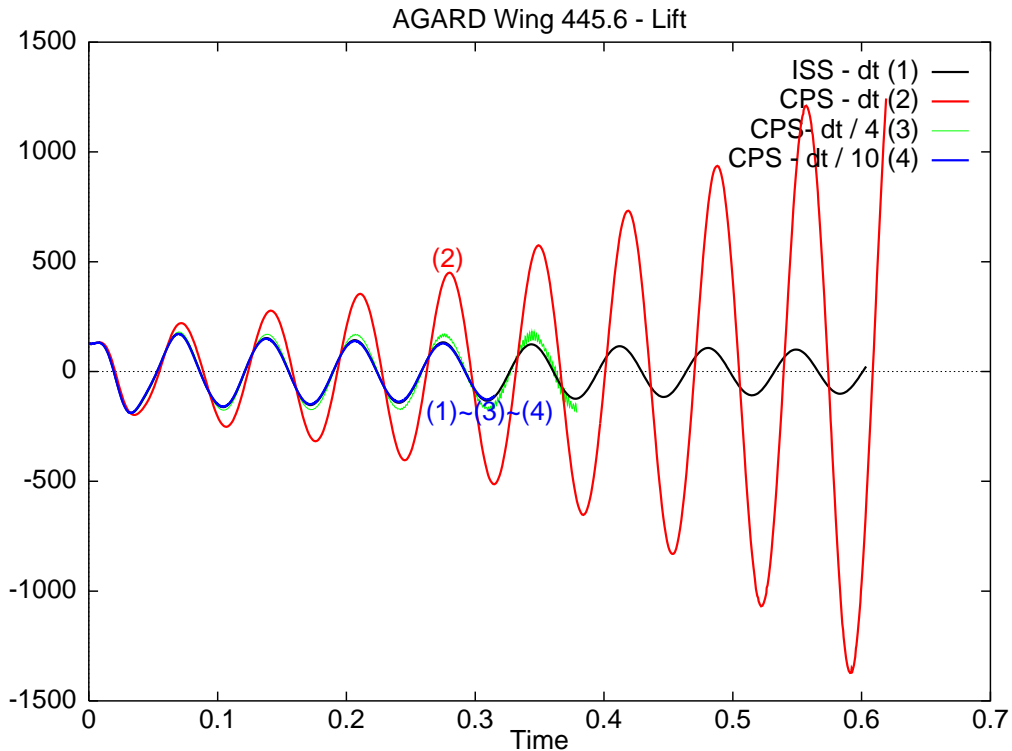
Figure 11: Comparison of lift histories with ISS and CPS.

this technique in some promising directions like non-matching interface discretizations, other non-conservative formulations. At the same time, this technique will help us to build new accurate and efficient coupling algorithms, since accuracy in boundary energy exchanges often goes on a par with extended global accuracy and stability domains for the partitioned procedure.

References

[1] G.P. Guruswamy. Interaction of Fluids and Structures for Aircraft Applications. *Computers & Structures*, 30(1/2): 1–13 , 1988.

[2] C. Farhat, M. Lesoinne, and N. Maman. Mixed eplicit/implicit time integration of coupled aeroelastic problems: three field formulation, geometric conservation and distributed solution. *International Journal for Numerical Methods in Fluids*, 21:807–835, 1995.

[3] S. Piperno. *Simulation numérique de phénomènes d'interaction fluide-structure*. PhD thesis, Ecole Nationale des Ponts et Chaussées, France, june 1995.

[4] S. Piperno, C. Farhat, and B. Larrouturou. Partitioned procedures for the transient solution of coupled aeroelastic problems. *Computer Methods in Applied Mechanics and Engineering*, 124(1-2):79–112, 1995.

[5] S. Piperno. Explicit/implicit fluid/structure staggered procedures with a structural predictor and fluid subcycling for 2d inviscid aeroelastic simulations. *International Journal for Numerical Methods in Fluids*, 25:1207–1226, 1997.

[6] C. Farhat and M. Lesoinne. Improved Staggered Algorithms for the Serial and Parallel Solution of Three-Dimensional Nonlinear Transient Aeroelastic Problems. Center for Aerospace Structures - 97-11, University of Colorado, Boulder, Colorado, June 1997. In review in AIAA Journal.

[7] P.D. Thomas and C.K. Lombard. Geometric Conservation Law and Its Application to Flow Computations on Moving Grids. *AIAA Journal*, 17:1030–1037, Oct 1979.

[8] R.L. Bisplinghoff, H. Ashley, and R.L. Halfman. *Aeroelasticity*. Addison-Wesley, Reading, MA, Nov 1957.

[9] J. C. Houbolt. A study of several aerothermoelastic problems of aircraft structures. Mitteilung aus dem Institut für Flugzeugstatik und Leichtbau 5, E.T.H., Zurich, 1958.

[10] B. Van Leer. Towards the Ultimate Conservative Difference Scheme V: a Second-Order Sequel to Godunov's Method. *Journal of Computational Physics*, 32:361–370, 1979.

[11] L. Fezoui and B. Stoufflet. A class of implicit upwind schemes for Euler simulations with unstructured meshes. *Journal of Computational Physics*, 84:174–206, 1989.

[12] C. Farhat, L. Fezoui, and S. Lantéri. Two-dimensional viscous flow computations on the Connection Machine: unstructured meshes, upwind schemes and massively parallel computations. *Computer methods in Applied Mechanics and Engineering*, 102:61–88, 1991.

[13] B. N'Konga and H. Guillard. Godunov Type Method on Non-Structured Meshes for Three-Dimensional Moving Boundary Problems. *Computer Methods in Applied Mechanics and Engineering*, 113:183–204, 1994.

[14] C. Farhat and M. Lesoinne. On the Accuracy, Stability, and Performance of the Solution of Three-Dimensional Nonlinear Transient Aeroelastic Problems by Partitioned Procedures. In *37th AIAA/ASME/ASCE/AHS/ASC Structures, Structural Dynamics and materials Conference, Salt lake City, Utah*, April 18-19 1996. AIAA paper 96-1388.

[15] M. Lesoinne and C. Farhat. Geometric conservation laws for flow problems with moving boundaries and deformable meshes, and their impact on aeroelastic computations. *Computer Methods in Applied Mechanics and Engineering*, (134):71–90, 1996.

Liste des derniers rapports de recherche du CERMICS

List of previous CERMICS research reports

97-93	N. Prcovic	*Distribution en escalier pour le développement en parallèle de l'arbre de recherche des CSP.* 16 pages, février 1997, Sophia-Antipolis
97-94	E. Cances B. Mennucci	*New applications of integral equations methods for solvation continuum models : ionic solutions and liquid crystals.* 21 pages, février 1997, Champs-sur-Marne
97-95	A.A.Burov D.Chevallier	*On motion of a rigid body about a fixed point with respect to the rotating frame.* 16 pages, février 1997, Champs-sur-Marne
97-96	K. Hao	*Dual number method, rank of a screw system and generation of Lie sub-algebras.* 25 pages, février 1997, Champs-sur-Marne
97-97	S. Cohen S. Rossignol	*Sharp asymptotics for the KPP's equation with geometric and irregular initial condition.* 11 pages, avril 1997, Champs-sur-Marne
97-98	F. Alliot C. Amrouche	*Problème de Stokes dans $\mathbf{R}^n$ et espaces de Sobolev avec poids.* 29 pages, avril 1997, Champs-sur-Marne
97-99	A. Toubol	*Small random perturbation of a classical mean field model.* 28 pages, avril 1997, Champs-sur-Marne
97-100	Numéro spécial	à paraître.

97-101	J.P. Cioni, M. Remaki	*Comparaison de deux méthodes de volumes finis en électromagnétisme.* 26 pages, mai 1997, Sophia-Antipolis
97-102	J.P. Lebacque	*Note sur le calcul des solutions du modèle LWR avec condition initiale $K > K_{max}$.* 26 pages, mai 1997, Champs-sur-Marne
97-103	D.P. Chevallier, S. Payandeh	*On Computation of Grasping Forces in Dynamic Manipulation Using a Three-Fingered Grasp.* 26 pages, mai 1997, Champs-sur-Marne
97-104	M. Jaume	*Explicit proofs of well-know results in logic programming.* 29 pages, juin 1997, Champs-sur-Marne
97-105	J. F. Pommaret, A. Quadrat	*Generalized bezout identity.* 14 pages, juin 1997, Champs-sur-Marne
97-106	Yi-Jun Xiao	*Some geometric and combinatorial properties of (0,m,2)-nets in base $b \geq 2$.* 14 pages, juin 1997, Champs-sur-Marne
97-107	C. Farhat S. Piperno	*Design and evaluation of staggered partitioned procedures for fluid-structure interaction simulations.* 21 pages, août 1997, Sophia-Antipolis

Ces rapports peuvent être obtenus en s'adressant au secrétariat du CERMICS :
The reports can be asked from:

Imane HAMADE
ENPC-CERMICS
6 et 8 Avenue Blaise Pascal
Cité Descartes Champs-sur-Marne
77455-Marne-La-Vallée CEDEX 2
Tél : (33) 01 - 64-15-35-71
email: hamade@cermics.enpc.fr